Structure and deformations of strongly magnetized neutron stars with twisted-torus configurations

R. Ciolfi,★ V. Ferrari★ and L. Gualtieri★

Dipartimento di Fisica 'G.Marconi', Sapienza Università di Roma and Sezione INFN ROMA1, 00185 Roma, Italy

ABSTRACT

We construct general relativistic models of stationary, strongly magnetized neutron stars. The magnetic field configuration, obtained by solving the relativistic Grad–Shafranov equation, is a generalization of the *twisted-torus* model recently proposed in the literature; the stellar deformations induced by the magnetic field are computed by solving the perturbed Einstein's equations; stellar matter is modelled using realistic equations of state. We find that in these configurations the poloidal field dominates over the toroidal field and that, if the magnetic field is sufficiently strong during the first phases of the stellar life, it can produce large deformations.

Key words: gravitational waves – stars: magnetic field – stars: neutron.

1 INTRODUCTION

After the discovery of the soft gamma repeaters and anomalous X-ray pulsars (Mazets et al. 1979; Mereghetti & Stella 1995), a model of these sources was proposed according to which they are neutron stars with a very strong magnetic field; these *magnetars* would have a surface field as large as $\sim 10^{14}$–10^{15} G, and internal fields about 10 times larger (Duncan & Thompson 1992). However, a clear picture of the structure, dynamics and evolution of magnetars is still missing. For instance we do not know whether the toroidal components of the field prevail on poloidal ones and how intense they are. Consequently, we do not know how large the deformation induced by the magnetic field on the star is, an information which is essential if one is interested in the gravitational wave emission of these sources. A deeper knowledge of the structure of strongly magnetized neutron stars would also help understanding various astrophysical processes involving magnetars (intense activity in the X-ray and gamma-ray spectra, quasi-periodic oscillations and eventually gamma-ray bursts).

In a recent paper (Ciolfi et al. 2009), to be referred to as Paper I hereafter, we constructed stationary models of non-rotating neutron stars endowed with a strong magnetic field, in the framework of general relativity (GR). In these models the poloidal field extends throughout the star and in the exterior, whereas the toroidal field is confined into a torus-shaped region inside the star, where the field lines are closed. It is worth reminding that these *twisted-torus* configurations have been found to be a quite general outcome of dynamical simulations of the early evolution of magnetized stars, in the framework of Newtonian gravity. Furthermore, due to magnetic

helicity conservation, they appear to be stable on dynamical time-scales (Braithwaite & Spruit 2004; Braithwaite & Nordlund 2006; Braithwaite & Spruit 2006), are not significantly affected by rotation (Yoshida, Yoshida & Eriguchi 2006), and do not depend on the initial angle between the rotation and the magnetic axes (Geppert & Rheinhardt 2006).

In Lander & Jones (2009) twisted-torus configurations were studied in Newtonian gravity; the maximal relative strength of the toroidal and poloidal components and the induced stellar deformation were evaluated using a polytropic equation of state (EOS) to model neutron star matter.

In Paper I, we studied the twisted-torus configurations in GR, including the contributions of higher order multipoles, and using a more realistic EOS. We considered a relation between the poloidal and the toroidal components of the field which is linear in the flux function, and estimated their ratio by determining the configuration of minimal energy at fixed magnetic helicity, under the assumption that the contribution of the $l > 1$ multipoles is minimum outside the star.

In this paper, we reconsider the above assumptions: the higher multipole contribution is not assumed a priori to be minimum outside the star, and we allow for a more general parametrization of the relation between toroidal and poloidal fields. We determine the configuration of minimal energy at fixed magnetic helicity, and evaluate the stellar deformations induced by the twisted-torus field by solving the perturbed Einstein equations including all relevant higher order multipoles.

As in Paper I, the magnetized fluid is described in the framework of ideal magnetohydrodynamics (MHD), which is accurate only in the first few hours of the star life when the crust is still liquid and the matter in the core has not yet undergone a phase transition to the superfluid state. Since the characteristic Alfvèn time is of the order of ~ 0.01–10 s, the magnetized fluid could reach a stationary state while the matter is still liquid and not yet

★E-mail: riccardo.ciolfi@roma1.infn.it (RC); valeria.ferrari@roma1.infn.it (VF); leonardo.gualtieri@roma1.infn.it (LG)

superfluid.[1] The magnetic field induces quadrupolar deformation on the stellar shape and, as we shall later show, for magnetic fields as high as those observed in magnetars this deformation would be large; when the crust forms, it would maintain this deformed shape. The magnetic field would subsequently evolve on time-scales of the order of $\sim 10^3$–10^5 yr due to dissipative effects like Ohmic decay, ambipolar diffusion and Hall drift (Goldreich & Reisenegger 1992; Woods & Thompson 2006; Pons & Geppert 2007).

The structure of the paper is as follows. In Section 2 we generalize the twisted-torus magnetic field configurations introduced in Paper I by dropping the assumption that the contribution from the $l > 1$ multipoles outside the star is minimum, and using a more general parametrization of the functional relation between toroidal and poloidal fields. In Section 3 we determine the stellar deformations induced by the magnetic field. In Section 4 we draw our conclusions.

2 TWISTED-TORUS MAGNETIC FIELD CONFIGURATION

In this section we briefly describe the formalism and the basic equations we solve to determine the twisted-torus magnetic field configuration; furthermore, we discuss the modifications introduced with respect to the analysis carried out in Paper I.

2.1 The model

We assume that the magnetized star is non-rotating, stationary and axisymmetric. The magnetized fluid is described in the framework of ideal MHD, in which the effects of electrical conductivity are neglected. Furthermore, we assume a vacuum exterior. We follow the same notation and conventions as in Paper I. We treat the magnetic field as a stationary, axisymmetric perturbation of a spherically symmetric background with metric

$$ds^2 = -e^{\nu(r)}dt^2 + e^{\lambda(r)}dr^2 + r^2(d\theta^2 + \sin^2\theta d\phi^2), \tag{1}$$

where $\nu(r)$ and $\lambda(r)$ are solutions of the unperturbed Einstein equations; the unperturbed four-velocity is $u^\mu = (e^{-\nu/2}, 0, 0, 0)$.

To model neutron star matter in the core we use the Akmal, Pandharipande, Ravenhall EOS, named APR2 (Akmal, Pandharipande & Ravenhall 1998), and the Glendenning EOS named GNH3 (Glendenning 1985); the crust is modelled using a standard EOS which accounts for the density–pressure relation in the crustal region, but not for its elastic properties (see Benhar, Ferrari & Gualtieri 2004). For a neutron star with mass $M = 1.4\,M_\odot$, the APR2 star has a large compactness ($R = 11.58$ km), whereas the compactness of the GNH3 star is small ($R = 14.19$ km).

As shown in Colaiuda et al. (2008), an appropriate gauge choice allows us to write the potential A_μ, in terms of which the Maxwell tensor ($F_{\mu\nu} = \partial_\nu A_\mu - \partial_\mu A_\nu$) is written as

$$A_\mu = \left(0, e^{(\lambda-\nu)/2}\Sigma, 0, \psi\right); \tag{2}$$

the two functions $\Sigma(r, \theta)$ and $\psi(r, \theta)$ describe the toroidal and the poloidal fields, respectively. Here A_μ is considered as a first-order quantity, $O(B)$. Furthermore, the ϕ-component of Euler's

equation yields $-\psi_{,r}J^r - \psi_{,\theta}J^\theta = O(B^4)$. Using Maxwell's equations and neglecting higher order terms one finds the integrability condition

$$\left(\sin\theta\,\Sigma_{,\theta}\right)_{,\theta}\psi_{,r} - \left(\sin\theta\,\Sigma_{,\theta}\right)_{,r}\psi_{,\theta} = 0, \tag{3}$$

which implies that $\sin\theta\,\Sigma_{,\theta}$ is a function of ψ:

$$\sin\theta\,\Sigma_{,\theta} \equiv \beta(\psi) = \zeta(\psi)\psi. \tag{4}$$

The function $\zeta(\psi) = \beta(\psi)/\psi$ represents the ratio between the toroidal and poloidal components of the magnetic field and characterizes the kind of field configuration we want to model. For instance, configurations with $\zeta = $ constant have been studied in Ioka & Sasaki (2004), Colaiuda et al. (2008) and Haskell et al. (2008). If the space outside the star is assumed to be vacuum, the toroidal field, and consequently ζ, must vanish for $r > R$, where R is the neutron star radius; in this case, the choice $\zeta = $ constant yields an inconsistency, unless one assumes that surface currents cancel the toroidal field outside the star, or imposes that the constant ζ assumes very particular values.

These problems do not arise with the twisted-torus configurations [see for instance Paper I or Lander & Jones (2009), Yoshida et al. (2006)] since the toroidal field is confined in a region inside the neutron star, and the magnetic field is continuous everywhere. For these configurations the function $\beta(\psi)$ is continuous, and has the form

$$\beta(\psi) \sim \Theta(|\psi/\bar\psi| - 1), \tag{5}$$

where $\bar\psi \equiv \psi(R, \pi/2)$ is the value of function ψ, which describes the poloidal field, on the stellar surface, and Θ is the Heaviside step function. If $\beta(\psi)$ satisfies equation (5), the magnetic field

$$B^\mu = \left[0, \frac{e^{-\lambda/2}}{r^2\sin\theta}\psi_{,\theta}, -\frac{e^{-\lambda/2}}{r^2\sin\theta}\psi_{,r}, -\frac{e^{-\nu/2}\beta(\psi)}{r^2\sin^2\theta}\right] \tag{6}$$

for $r > R$ becomes purely poloidal, consistently with the assumption of vacuum outside the star.

To find the field configuration we need to solve the relativistic Grad–Shafranov (GS) equation, which follows from Euler's and Maxwell's equations (see Paper I for details) and has the form

$$-\frac{e^{-\lambda}}{4\pi}\left[\psi'' + \frac{\nu'-\lambda'}{2}\psi'\right] - \frac{1}{4\pi r^2}\left[\psi_{,\theta\theta} - \cot\theta\,\psi_{,\theta}\right]$$
$$-\frac{e^{-\nu}}{4\pi}\beta\frac{d\beta}{d\psi} = (\rho + P)r^2\sin^2\theta[c_0 + c_1\psi]. \tag{7}$$

The constants c_0, c_1 characterize the ϕ-component of the current density inside the star, which has the form

$$J_\phi = \frac{e^{-\nu}}{4\pi}\beta\frac{d\beta}{d\psi} + (\rho + P)r^2\sin^2\theta[c_0 + c_1\psi + O(B^2)]. \tag{8}$$

If we now define $\psi(r, \theta) \equiv \sin\theta\, a(r, \theta)_{,\theta}$, expand the function $a(r, \theta)$ in Legendre polynomials

$$a(r, \theta) = \sum_{l=1}^{\infty} a_l(r)P_l(\cos\theta) \tag{9}$$

and project the GS equation on to the different harmonic components, we find a system of coupled ordinary differential equations for the functions $a_l(r)$. These equations are solved by imposing the following boundary conditions. (i) The functions $a_l(r)$ have a regular behaviour at the origin; an asymptotic expansion of the GS equation shows that this implies

$$a_l(r \to 0) = \alpha_l r^{l+1}. \tag{10}$$

---

[1] We remark that even in presence of a stable stratification of the chemical composition, a magnetic field as strong as $B \gtrsim 10^{15}$ is still allowed to evolve throughout the star on a dynamical time-scale (Thompson & Murray 2001).

(ii) The functions $a_l(r)$ and their derivatives $a_l'(r)$ are continuous across the stellar surface where they match with the solutions in vacuum, which are known in an analytical form (see Paper I); therefore, the ratios a_l'/a_l computed at $r = R$ in terms of the interior and exterior numerical solutions must coincide. (iii) The overall normalization of the field is fixed by requiring the $l = 1$ component of the magnetic field at the pole to be $B_{\mathrm{pole}} = 10^{16}$ G; this corresponds to $a_1(R) = 1.93 \times 10^{-2}$ km.

Once the form of the function $\beta(\psi)$ and the number n of multipoles we want to include have been assigned, the field is determined when we fix $n + 2$ arbitrary constants: the n constants α_l and the two constants c_0 and c_1 defined in equation (8). $n + 1$ of them are determined by imposing the boundary conditions. In Paper I the last constant was fixed assuming that the contribution of higher order multipoles outside the star is minimum, i.e. by minimizing the function $(\sum_{l>1} a_l^2)/a_1^2$, for $r \geq R$. In this paper we remove this assumption, thus exploring a larger parameter space, and fix the last constant by finding the configurations which are energetically favoured (this is discussed in detail in the next section).

To this purpose, we minimize the total energy at fixed magnetic helicity. As shown in Paper I, this is equivalent to minimize the ratio $\delta M / H_{\mathrm{m}}$, where H_{m} is the magnetic helicity,

$$H_{\mathrm{m}} = \frac{1}{2} \int \mathrm{d}^3 x \sqrt{-g} \epsilon^{0\beta\gamma\delta} F_{\gamma\delta} A_{\beta}, \tag{11}$$

and δM is the mass–energy increase due to the perturbation that the magnetic field induces on the spherical star. This quantity is determined in terms of the functions which characterize the far-field limit of the space–time metric. Finally, we compute the ratio of the magnetic energy stored in the poloidal field to the total magnetic energy, $E_{\mathrm{p}}/E_{\mathrm{m}}$. The equations to determine these quantities are given in Appendix B.

The GS system of equations admits two particular classes of solutions: the symmetric (with respect to the equatorial plane) solutions, with vanishing even-order components ($a_{2l} \equiv 0$), and the antisymmetric solutions, with vanishing odd-order components ($a_{2l+1} \equiv 0$). In Paper I the choice of minimizing the $l > 1$ multipole contribution led naturally to symmetric solutions, i.e. those with $a_{2l} \equiv 0$. It is worth noting that even-order multipoles contribute to the energy but not to the magnetic helicity; therefore, any solution minimizing energy at fixed magnetic helicity corresponds to a vanishing antisymmetric component. Since in this paper we still look for minimal energy configurations, we shall consider only symmetric solutions. In addition, as in Paper I, we shall restrict to multipoles with

$l \leq 5$ (the relevance of $l > 5$ multipoles is discussed in Paper I, section 5.3).

2.2 Relative strength of different multipoles

As explained in the previous section, since we remove the condition of minimal contribution from higher order multipoles, the boundary conditions are not sufficient to fix all the parameters of the problem and we are left with a free arbitrary constant. We choose c_1 as a 'free' parameter. In this section we shall choose the function $\beta(\psi)$ as in Paper I:

$$\beta(\psi) = \psi \zeta(\psi) = \psi \zeta_0 \left(|\psi/\bar{\psi}| - 1 \right) \Theta(|\psi/\bar{\psi}| - 1), \tag{12}$$

where ζ_0 is a real parameter. In the next section we shall consider a more general form of $\beta(\psi)$ compatible with equation (5). The constant ζ_0 determines the ratio between the amplitudes of the toroidal and poloidal fields. Thus, we minimize the energy with respect to two parameters: c_1 and ζ_0. We proceed as follows. For assigned values of ζ_0:

(i) we solve the equations for the a_l values for different values of c_1;

(ii) we compute $\delta M / H_{\mathrm{m}}$ – the quantity to minimize – for the corresponding configurations;

(iii) we compute the quantity $\sqrt{a_3^2(R) + a_5^2(R)}$, which represents the surface contribution of the multipoles higher than $l = 1$.

In Fig. 1 we plot the ratio $\delta M / H_{\mathrm{m}}$ as a function of $\sqrt{a_3^2(R) + a_5^2(R)}$. In the left-hand panel we fix $\zeta_0 = 0.61$ km^{-1}. In Paper I we showed that, under the assumption of minimal contribution of higher order multipoles, i.e.

$$\sqrt{a_3^2 + a_5^2} \qquad \text{minimum for} \quad r \geq R$$

[hereafter, this will be named the minimum high multipole (MHM) condition], the quantity $\delta M / H_{\mathrm{m}}$ is minimum for this value of ζ_0. This MHM configuration corresponds to the point A on the curve plotted in Fig. 1.

Since we now drop the MHM condition, the minimum of $\delta M / H_{\mathrm{m}}$ occurs for a different value of $\sqrt{a_3^2(R) + a_5^2(R)}$ (point B in Fig. 1), which corresponds to the energetically favoured configuration for $\zeta_0 = 0.61$ km^{-1}. For an assigned value of H_{m}, the relative variation of the total energy of the configuration B with respect to A is of the order of 13 per cent. Fig. 1 refers to a star with EOS APR2. Similar results are obtained for the GNH3 star.

In the right-hand panel of Fig. 1 we plot $\delta M / H_{\mathrm{m}}$ for selected values of ζ_0, and compare the different profiles. We have explored
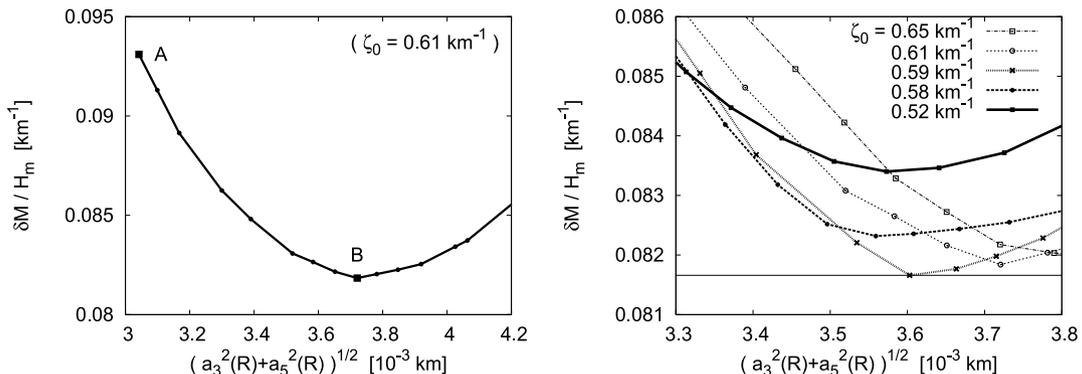
Figure 1. The function $\delta M/H_{\mathrm{m}}$ is plotted as a function of $\sqrt{a_3^2(R) + a_5^2(R)}$: on the left-hand panel $\zeta_0 = 0.61$ km^{-1}, on the right-hand panel the cases $\zeta_0 = 0.65$, 0.61, 0.59, 0.58 and 0.52 km^{-1} are shown together for comparison.
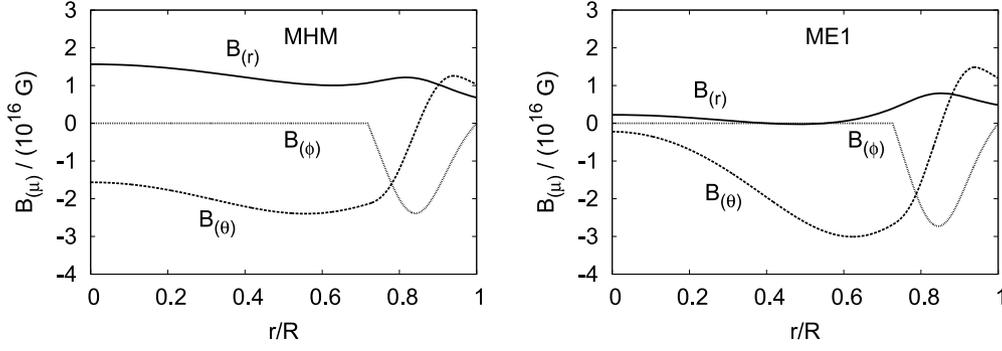
Figure 2. The profiles of the tetrad components of the magnetic field $B_{(r)}(\theta = 0)$, $B_{(\theta)}(\theta = \pi/2)$, $B_{(\phi)}(\theta = \pi/2)$ are plotted as functions of the radial distance normalized to the stellar radius. The left-hand panel refers to the MHM configuration (energy is minimized assuming that the contribution of the multipoles higher than $l = 1$ is minimum for $r > R$); in this case $\zeta_0 = 0.61$ km^{-1}. The right-hand panel refers to the minimal energy configuration ME1, obtained with no assumption on the relative strengths of the different multipoles, and for $\zeta_0 = 0.59$ km^{-1}.

the parameter space (ζ_0, $\sqrt{a_3^2(R) + a_5^2(R)}$)[equivalent to ($\zeta_0$, c_1)], finding that the function $\delta M/H_m$ has a minimum ($\delta M/H_m = 0.0817$) for $\zeta_0 = 0.59$ km^{-1} and $\sqrt{a_3^2(R) + a_5^2(R)} = 3.6 \times 10^{-3}$ km. It is worth reminding that the $l = 1$ contribution is $a_1(R) = 1.93 \times 10^{-2}$ km. We shall refer to this configuration as the minimal energy 1 (ME1) configuration.

In Fig. 2 we compare the profiles of the tetrad components of the magnetic field for the MHM and the ME1 configurations. We see that, whereas for the MHM configuration $B_{(\theta)}$ and $B_{(r)}$ are significantly different from zero throughout the star, for the ME1 configuration, obtained with no assumption on the relative strengths of the different multipoles for $r > R$, these field components are strongly reduced near the axis. Conversely, the toroidal component $B_{(\phi)}$ has a similar behaviour in both configurations. The two panels of Fig. 2 illustrate how the magnetic field rearranges inside the star when the MHM condition is removed. The situation can be explained as follows. The magnetic helicity H_m can be written as

$$H_m = -2\pi \int_0^R \mathrm{d}r \int_0^\pi (A_r \psi_{,\theta} - \psi A_{r,\theta}) \, \mathrm{d}\theta; \tag{13}$$

therefore, H_m vanishes if either $\psi = 0$, i.e. the poloidal field vanishes, or $A_r = 0$, i.e. the toroidal field vanishes. In the twisted-torus model the toroidal field is zero in the inner part of the star; therefore H_m receives contributions only from the magnetic field in the region where $B_{(\phi)} \neq 0$. Since in that region the field components of the MHM and ME1 configurations are similar, these configurations have nearly the same magnetic helicity H_m. On the other hand, the energy δM receives contributions from the field components throughout the entire star, and these contributions are not vanishing in the region where $B_{(\phi)} = 0$. When we minimize the function $\delta M/H_m$ in the ME1 configuration, the $l > 1$ multipoles, which were kept minimum in the MHM configuration, do not change H_m significantly, but they change δM, and since we require δM to be minimum, they combine as to reduce the field in the inner region of the star.

2.3 A more general choice of the function $\beta(\psi)$

In this section we construct twisted-torus configurations, choosing two different forms of the function β, namely

$$\beta(\psi) = \psi \zeta_0 \left(|\psi/\bar{\psi}| - 1\right)^\sigma \Theta(|\psi/\bar{\psi}| - 1) \tag{14}$$

(note that $\sigma = 1$ corresponds to equation 12), and

$$\beta(\psi) = -\beta_0 \left(|\psi/\bar{\psi}| - 1\right)^\sigma \Theta(|\psi/\bar{\psi}| - 1), \tag{15}$$

where β_0 is a constant of order $O(B)$. A choice similar to (14) has been considered by Lander & Jones (2009), who have studied the field configurations in a Newtonian framework. Although equations (14) and (15) do not exhaust all possible choices of the function $\beta(\psi)$, they are general enough to capture the main features of the stationary twisted-torus configurations.

For β given by equation (14) the magnetic field components and the GS equation are

$$B^\mu = \left(0, \; \frac{\mathrm{e}^{-\lambda/2}}{r^2 \sin\theta} \psi_{,\theta}, \; -\frac{\mathrm{e}^{-\lambda/2}}{r^2 \sin\theta} \psi_{,r}, \right.$$
$$\left. -\frac{\mathrm{e}^{-\nu/2} \zeta_0 \psi \left(|\psi/\bar{\psi}| - 1\right)^\sigma}{r^2 \sin^2\theta} \Theta(|\psi/\bar{\psi}| - 1) \right) \tag{16}$$

and

$$-\frac{\mathrm{e}^{-\lambda}}{4\pi} \left[\psi'' + \frac{\nu' - \lambda'}{2} \psi' \right] - \frac{1}{4\pi r^2} \left[\psi_{,\theta\theta} - \cot\theta \, \psi_{,\theta} \right]$$
$$-\frac{\mathrm{e}^{-\nu} \zeta_0^2}{4\pi} \psi \left[\left(|\psi/\bar{\psi}| - 1\right)^{2\sigma} + \sigma |\psi/\bar{\psi}| \left(|\psi/\bar{\psi}| - 1\right)^{2\sigma - 1} \right]$$
$$\times \Theta(|\psi/\bar{\psi}| - 1)$$
$$= (\rho + P) r^2 \sin^2\theta [c_0 + c_1 \psi]. \tag{17}$$

For β given by equation (15) they are

$$B^\mu = \left(0, \; \frac{\mathrm{e}^{-\lambda/2}}{r^2 \sin\theta} \psi_{,\theta}, \; -\frac{\mathrm{e}^{-\lambda/2}}{r^2 \sin\theta} \psi_{,r}, \right.$$
$$\left. \frac{\mathrm{e}^{-\nu/2} \beta_0 \left(|\psi/\bar{\psi}| - 1\right)^\sigma}{r^2 \sin^2\theta} \Theta(|\psi/\bar{\psi}| - 1) \right) \tag{18}$$

and

$$-\frac{\mathrm{e}^{-\lambda}}{4\pi} \left[\psi'' + \frac{\nu' - \lambda'}{2} \psi' \right] - \frac{1}{4\pi r^2} \left[\psi_{,\theta\theta} - \cot\theta \, \psi_{,\theta} \right]$$
$$-\frac{\mathrm{e}^{-\nu} \beta_0^2}{4\pi \psi} \sigma |\psi/\bar{\psi}| \left(|\psi/\bar{\psi}| - 1\right)^{2\sigma - 1} \Theta(|\psi/\bar{\psi}| - 1)$$
$$= (\rho + P) r^2 \sin^2\theta [c_0 + c_1 \psi]. \tag{19}$$

The field configurations are now identified by three parameters: (σ, c_1, ζ_0) for choice (14), and (σ, c_1, β_0) for choice (15). As in the previous section, we look for the minimal energy configuration at fixed magnetic helicity; furthermore, we compute the ratio of the poloidal magnetic energy to the total magnetic energy. We solve the system of GS equations for $l = 1, 3, 5$ (they are given in Appendix A for both cases), with the boundary conditions discussed
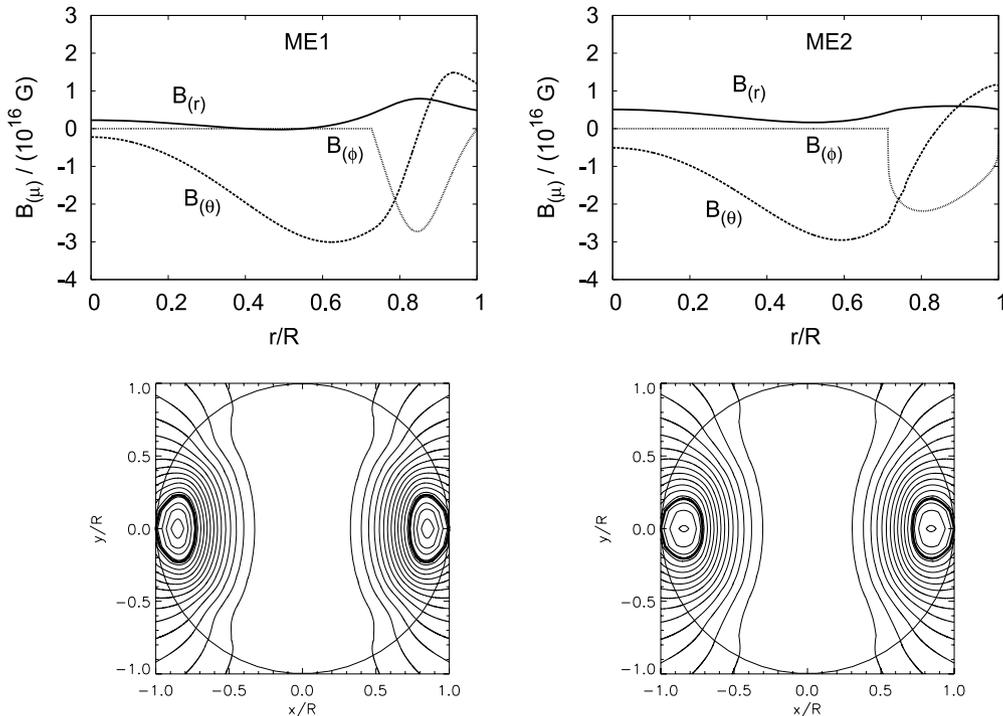
Figure 3. The profiles of the tetrad components of the magnetic field $[B_{(r)}(\theta = 0),\ B_{(\theta)}(\theta = \pi/2),\ B_{(\phi)}(\theta = \pi/2)]$ are shown (upper panels). In the lower panels we show the projection of the field lines in the meridional plane. Left- and right-hand panels refer, respectively, to the configuration ME1 and ME2.

in Section 2.1. For each configuration we compute the magnetic helicity $H_{\rm m}$, the correction to the total energy δM and the poloidal and toroidal contributions to the magnetic energy $E_{\rm m}$. The equations to determine δM and $E_{\rm m}$ are given in Appendix B. The energetically favoured configurations are found by minimizing $\delta M / H_{\rm m}$ with respect to the three parameters.

Let us first consider the case in which the relation between toroidal and poloidal fields is given by equation (14). We find that the minimal energy configuration (for the APR2 EOS) corresponds to

$$\sigma = 0.18, \quad \zeta_0 = 0.20 \, \text{km}^{-1},$$
$$\sqrt{a_3^2(R) + a_5^2(R)} = 3.4 \times 10^{-3} \, \text{km}. \tag{20}$$

We shall refer to this configuration as the ME2 configuration. In Fig. 3 the configurations with $\sigma = 1$ (ME1) and $\sigma = 0.18$ (ME2) are compared. In ME2 the magnetic field has a slightly different shape: in particular, the toroidal component is larger near the surface of the star, and the extension of the toroidal field region along the y-axis is smaller. The ratio of the poloidal magnetic energy to the total magnetic energy inside the star is

$$E_{\rm p}/E_{\rm m} = 0.91 \quad \text{for ME1},$$
$$E_{\rm p}/E_{\rm m} = 0.87 \quad \text{for ME2}.$$

If, as in Paper I, we include also the exterior field we find $E_{\rm p}/E_{\rm m} = 0.93,\ 0.90$, respectively, for the configurations ME1 and ME2. Furthermore, we find that the minimal energy configuration is nearly the configuration with smaller ratio $E_{\rm p}/E_{\rm m}$, i.e. with larger toroidal component (confirming the results of Paper I): thus, the $\sigma = 0.18$ case also corresponds to the minimum value of $E_{\rm p}/E_{\rm m}$ which can be obtained with choice (14). We can conclude that if σ is not assumed to be 1, we can obtain configurations with a larger toroidal contribution, but only by a small amount.
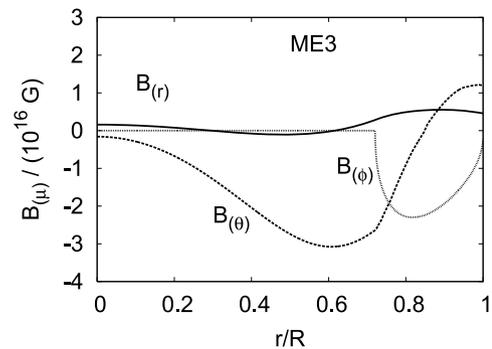
Figure 4. The profiles of the tetrad components of the magnetic field are shown for the configuration ME3, corresponding to β given by equation (15); the values of the parameters are given in equation (21).

We now consider choice (15) for the function β. In this case the minimal energy configuration (for the APR2 EOS) corresponds to

$$\sigma = 0.42, \quad \beta_0 = 9 \times 10^{-4},$$
$$\sqrt{a_3^2(R) + a_5^2(R)} = 3.7 \times 10^{-3} \, \text{km}. \tag{21}$$

This configuration, which is shown in Fig. 4, will be referred to as the ME3 configuration. A comparison with the right-hand panel of Fig. 3 shows that the ME2 and ME3 configurations are very similar. Inside the star $E_{\rm p}/E_{\rm m} = 0.88$ and, as in the previous case, it is the minimum value which can be obtained for this choice of the function β.

For the GNH3 EOS, we obtain similar results. The minimal energy configuration is obtained with choice (14), and

$$\sigma = 0.30, \quad \zeta_0 = 0.13 \, \text{km}^{-1},$$
$$\sqrt{a_3^2(R) + a_5^2(R)} = 5.1 \times 10^{-3} \, \text{km}. \tag{22}$$

The ratio of the poloidal energy to the total magnetic energy inside the star, for this configuration, is $E_p/E_m = 0.93$.

We conclude that when we allow for a non-minimal contribution of the $l > 1$ multipoles and for a more general parametrization of the function $\beta(\psi)$, the magnetic field changes with respect to the MHM configuration found in Paper I as follows: the poloidal field near the axis of the star is smaller, and the toroidal field near the stellar surface is larger. In all cases the toroidal field never contributes to more than ~13 per cent of the total magnetic energy stored inside the star.

3 STRUCTURE DEFORMATIONS

In this section we compute the quadrupole deformation induced by the magnetic field for the twisted-torus configurations previously obtained. To this purpose we solve Einstein's equations with a perturbative approach: the magnetic field and the deformations it induces are considered as perturbations of a static, spherically symmetric background. The relevant equations are described in Appendix C. The quantity which is relevant to estimate the gravitational wave emission of the deformed star is the quadrupole ellipticity

$$\varepsilon_Q = \frac{Q}{I}, \qquad (23)$$

where Q is the mass–energy quadrupole moment (see equation C2), and I the mean value of the star's moment of inertia. Indeed, if the star rotates about an axis misaligned with the symmetry (or magnetic) axis with a wobble angle α, it emits gravitational waves with amplitude (Bonazzola & Gourgoulhon 1996)

$$h_0 \simeq \frac{4G}{rc^4} \Omega^2 I |\varepsilon_Q| \sin \alpha, \qquad (24)$$

where Ω is the star angular velocity. We remind that we normalize the magnetic field by fixing its value at the pole as $B_{pole} = 10^{16}$ G (see Section 2), and that the quadrupole ellipticity scales as B_{pole}^2.

Furthermore, it is interesting to determine the sign of the quadrupole ellipticity because, if $\varepsilon_Q < 0$ (corresponding to a prolate shape), a 'spin-flip' mechanism associated to viscous forces may arise, as suggested in Jones (1975) and Cutler (2002). In this scenario, the angle between the magnetic axis and the rotation axis would grow on a dissipation time-scale, until they become orthogonal, and this process would be associated to a large gravitational wave emission, potentially detectable by the advanced generation of ground-based detectors Virgo and LIGO.

It is well known that while the poloidal field tends to make the star oblate, the toroidal field tends to make it prolate. Since in our configurations the poloidal field dominates over the toroidal one, ε_Q is always positive. Therefore, twisted-torus configurations are not compatible with the spin-flip mechanism, and $|\varepsilon_Q|$ is larger for configurations in which the toroidal contribution is smaller. We find that, for the APR2 EOS, $\varepsilon_Q = 3.5 \times 10^{-4}$ and 3.7×10^{-4}, respectively, for the ME2 and ME3 configurations.

It is also interesting to consider twisted-torus configurations which do not correspond to minimal energy. Indeed, it is not guaranteed that the star sets in the minimal energy configuration before the crust forms and the stellar matter becomes superfluid. Therefore, we have determined the entire range of possible ellipticities for the twisted-torus configurations analysed in this paper; we find $3.5 \times 10^{-4} \lesssim \varepsilon_Q \lesssim 4.8 \times 10^{-4}$ for the APR2 EOS, and $8.1 \times 10^{-4} \lesssim \varepsilon_Q \lesssim 9.6 \times 10^{-4}$ for the GNH3 EOS. As discussed above, the larger ellipticities are obtained in the purely poloidal limit, whereas the smaller ellipticities refer to the minimal energy configurations. We note that, as expected, given the mass ($1.4 \, M_\odot$ in our case), less
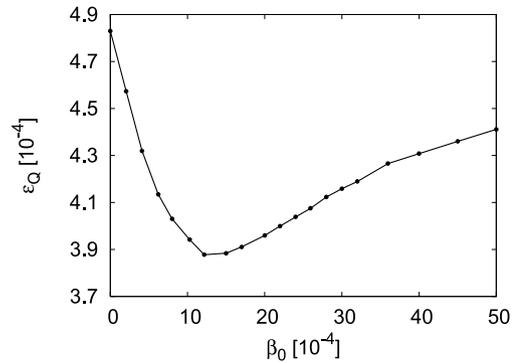
Figure 5. Ellipticities versus β_0 for $\sigma = 1$, with $\beta(\psi)$ given by (15).

compact stars (GNH3) have larger ellipticities. We also note that the values of ε_Q we find for the purely poloidal case are similar to the maximal ellipticity found in Lander & Jones (2009), where a polytropic EOS was employed.

Summarizing, the quadrupole ellipticity ε_Q corresponding to $B_{pole} = 10^{16}$ G would lie in the quite narrow ranges $(3.5, 4.8) \times 10^{-4}$ for the APR2 EOS and $(8.1, 9.6) \times 10^{-4}$ for the GNH3 EOS, i.e.

$$\varepsilon_Q \simeq k \left[\frac{B_{pole} \, (G)}{10^{16}} \right]^2 \times 10^{-4}, \qquad (25)$$

with $k \simeq 4$ for the APR2 EOS and $k \simeq 9$ for the GNH3 EOS.

As an example of the behaviour of ε_Q when the toroidal field contribution changes, in Fig. 5 we plot ε_Q versus the parameter β_0 for configurations obtained choosing $\beta(\psi)$ as in equation (15), assuming that $\sigma = 1$ and that the contribution of the $l > 1$ multipoles is fixed by energy minimization. In particular, we see that the maximal deformation is given by the purely poloidal configuration.

4 CONCLUDING REMARKS

In this paper we construct relativistic models of non-rotating, stationary stars, with a twisted-torus magnetic field configuration. We extend the work done in Paper I, by removing the assumption of minimal contribution from multipoles higher than $l = 1$, by considering more general forms of the function $\beta(\psi)$ which describes the ratio between toroidal and poloidal components, and by evaluating the deformation that the magnetic field induces on the star.

We find that the non-minimal contribution of the $l > 1$ multipoles, and the more general parametrization of the function β, yield some interesting differences with respect to the magnetic field configurations found in Paper I: the new configurations have a much smaller poloidal field near the symmetry axis, and a larger toroidal field near the stellar surface. In any event, the toroidal field never contributes to more than ~13 per cent of the total magnetic energy stored inside the star.

Since the poloidal field always prevails, in the twisted-torus configurations the quadrupole ellipticity of the star ε_Q is always positive, and its maximum value is obtained in the purely poloidal limit. As shown by equation (25), which summarizes our results on the stellar deformation, ε_Q depends on the EOS of matter: less compact stars can have larger deformations.

We remark that the ellipticities given by equation (25) are larger than the bounds derived by evaluating the maximal strain that the crust can sustain (Ushomirsky, Cutler & Bildsten 2000; Haskell, Jones & Andersson 2006). These bounds do not apply to the case we study, because in our case the magnetic field is assumed to

reach a stationary configuration during the first few seconds of the neutron star life, when the star is still fluid and no crust has formed yet; therefore, if the field is sufficiently strong, the deformation it induces can be large, and may persist as the star cools down and the crust freezes in a non-spherical shape (see also the discussion in Haskell et al. 2008 and Colaiuda et al. 2008).

Recent results from the LIGO–Virgo collaboration (Abbot et al. 2008, 2009) put an upper limit on the ellipticity of the Crab pulsar, which should be $\varepsilon_Q \lesssim 10^{-4}$. Our study indicates that strongly magnetized neutron stars with ellipticities of this order of magnitude may exist, provided this strong deformation was built up before the crust was formed, and the magnetic field was sufficiently strong.

In order to further substantiate this scenario, an important issue which remains to be clarified is whether the twisted-torus configurations we find are stable. This issue will be the subject of a future investigation.

ACKNOWLEDGMENTS

REFERENCES

Abbot B. et al., 2008, ApJ, 643, L45
Abbot B. et al., 2009, preprint (arXiv:0909.3583v3)
Akmal A., Pandharipande V. R., Ravenhall D. G., 1998, Phys. Rev. C, 58, 1804
Benhar O., Ferrari V., Gualtieri L., 2004, Phys. Rev. D, 70, 124015
Bonazzola S., Gourgoulhon E., 1996, A&A, 312, 1675
Braithwaite J., Nordlund Å., 2006, A&A, 450, 1077
Braithwaite J., Spruit H. C., 2004, Nat, 431, 819
Braithwaite J., Spruit H. C., 2006, A&A, 450, 1097
Ciolfi R., Ferrari V., Gualtieri L., Pons J. A., 2009, MNRAS, 397, 913 (Paper I)
Colaiuda A., Ferrari V., Gualtieri L., Pons J. A., 2008, MNRAS, 385, 2080
Cutler C., 2002, Phys. Rev. D, 66, 084025
Duncan R. C., Thompson C., 1992, ApJ, 392, L9
Geppert U., Rheinhardt M., 2006, A&A, 456, 639
Glendenning N. K., 1985, ApJ, 293, 470
Goldreich P., Reisenegger A., 1992, ApJ, 395, 250
Haskell B., Jones D. I., Andersson N., 2006, MNRAS, 373, 1423
Haskell B., Samuelsson L., Glampedakis K., Andersson N., 2008, MNRAS, 385, 531
Ioka K., Sasaki M., 2004, ApJ, 600, 296
Jones P. B., 1975, Astrophys. Space Sci., 33, 215
Lander S. K., Jones D. I., 2009, MNRAS, 395, 2162
Mazets E. P., Golentskii S. V., Ilinskii V. N., Aptekar R. L., Guryan Y. A., 1979, Nat, 282, 587
Mereghetti S., Stella L., 1995, ApJ, 442, L17
Misner C. W., Thorne K. S., Wheeler J. A., 1973, Gravitation. Freeman & Co., New York
Pons J. A., Geppert U., 2007, A&A, 470, 303
Straumann N., 2004, General Relativity. Springer-Verlag, Berlin, Heidelberg
Thompson C., Murray N., 2001, ApJ, 560, 339
Thorne K. S., 1980, Rev. Modern Phys., 52, 299
Ushomirsky G., Cutler C., Bildsten L., 2000, MNRAS, 319, 902
Woods P. M., Thompson C., 2006, in Cambridge Astrophysics Series Vol. 39, Compact Stellar X-ray Sources. Cambridge Univ. Press, Cambridge, p. 547
Yoshida S., Yoshida S., Eriguchi Y., 2006, ApJ, 651, 462

APPENDIX A: GS EQUATIONS

The harmonic expansion of the GS equations (17), corresponding to choice (14) of the function $\beta(\psi)$, gives (if we include the $l = 1, 3, 5$ components in the expansion)

$$
\frac{1}{4\pi} \left(e^{-\lambda} a_1'' + e^{-\lambda} \frac{\nu' - \lambda'}{2} a_1' - \frac{2}{r^2} a_1 \right)
$$
$$
- \frac{e^{-\nu}}{4\pi} \int_0^\pi (3/4)\, \zeta_0^2 \psi \left[\left(|\psi/\bar{\psi}| - 1 \right)^{2\sigma} \right.
$$
$$
\left. + \sigma |\psi/\bar{\psi}| \left(|\psi/\bar{\psi}| - 1 \right)^{2\sigma - 1} \right] \Theta(|\psi/\bar{\psi}| - 1) \sin\theta \, d\theta
$$
$$
= \left[c_0 - \frac{4}{5} c_1 \left(a_1 - \frac{3}{7} a_3 \right) \right] (\rho + P) r^2, \tag{A1}
$$

$$
\frac{1}{4\pi} \left(e^{-\lambda} a_3'' + e^{-\lambda} \frac{\nu' - \lambda'}{2} a_3' - \frac{12}{r^2} a_3 \right)
$$
$$
+ \frac{e^{-\nu}}{4\pi} \int_0^\pi (7/48)\, \zeta_0^2 \psi \left[\left(|\psi/\bar{\psi}| - 1 \right)^{2\sigma} \right.
$$
$$
\left. + \sigma |\psi/\bar{\psi}| \left(|\psi/\bar{\psi}| - 1 \right)^{2\sigma - 1} \right]
$$
$$
\times \Theta(|\psi/\bar{\psi}| - 1)(3 - 15\cos^2\theta) \sin\theta \, d\theta
$$
$$
= c_1 (\rho + P) r^2 \left(\frac{2}{15} a_1 - \frac{8}{15} a_3 + \frac{10}{33} a_5 \right), \tag{A2}
$$

$$
\frac{1}{4\pi} \left(e^{-\lambda} a_5'' + e^{-\lambda} \frac{\nu' - \lambda'}{2} a_5' - \frac{30}{r^2} a_5 \right)
$$
$$
+ \frac{e^{-\nu}}{4\pi} \int_0^\pi (11/60)\, \zeta_0^2 \psi \left[\left(|\psi/\bar{\psi}| - 1 \right)^{2\sigma} \right.
$$
$$
\left. + \sigma |\psi/\bar{\psi}| \left(|\psi/\bar{\psi}| - 1 \right)^{2\sigma - 1} \right]
$$
$$
\times \Theta(|\psi/\bar{\psi}| - 1) \frac{(-315\cos^4\theta + 210\cos^2\theta - 15)}{8} \sin\theta \, d\theta
$$
$$
= c_1 (\rho + P) r^2 \left(\frac{4}{21} a_3 - \frac{20}{39} a_5 \right), \tag{A3}
$$

where

$$
\psi = \left[-a_1 + \frac{a_3(3 - 15\cos^2\theta)}{2} \right.
$$
$$
\left. + \frac{a_5(-315\cos^4\theta + 210\cos^2\theta - 15)}{8} \right] \sin^2\theta. \tag{A4}
$$

The harmonic expansion of the GS equations (19), corresponding to choice (15) of the function $\beta(\psi)$, gives

$$
\frac{1}{4\pi} \left(e^{-\lambda} a_1'' + e^{-\lambda} \frac{\nu' - \lambda'}{2} a_1' - \frac{2}{r^2} a_1 \right)
$$
$$
- \frac{e^{-\nu}}{4\pi} \int_0^\pi (3/4)\, \frac{\beta_0^2}{\psi} \sigma |\psi/\bar{\psi}| \left(|\psi/\bar{\psi}| - 1 \right)^{2\sigma - 1}
$$
$$
\times \Theta(|\psi/\bar{\psi}| - 1) \sin\theta \, d\theta
$$
$$
= \left[c_0 - \frac{4}{5} c_1 \left(a_1 - \frac{3}{7} a_3 \right) \right] (\rho + P) r^2, \tag{A5}
$$

$$
\frac{1}{4\pi} \left(e^{-\lambda} a_3'' + e^{-\lambda} \frac{\nu' - \lambda'}{2} a_3' - \frac{12}{r^2} a_3 \right)
$$
$$
+ \frac{e^{-\nu}}{4\pi} \int_0^\pi (7/48)\, \frac{\beta_0^2}{\psi} \sigma |\psi/\bar{\psi}| \left(|\psi/\bar{\psi}| - 1 \right)^{2\sigma - 1}
$$
$$
\times \Theta(|\psi/\bar{\psi}| - 1)(3 - 15\cos^2\theta) \sin\theta \, d\theta
$$
$$
= c_1 (\rho + P) r^2 \left(\frac{2}{15} a_1 - \frac{8}{15} a_3 + \frac{10}{33} a_5 \right), \tag{A6}
$$

$$\frac{1}{4\pi}\left(e^{-\lambda}a_5'' + e^{-\lambda}\frac{\nu'-\lambda'}{2}a_5' - \frac{30}{r^2}a_5\right)$$

$$+\frac{e^{-\nu}}{4\pi}\int_0^\pi (11/60)\frac{\beta_0^2}{\psi}\sigma|\psi/\bar\psi|\left(|\psi/\bar\psi|-1\right)^{2\sigma-1}$$

$$\times\Theta(|\psi/\bar\psi|-1)\frac{(-315\cos^4\theta+210\cos^2\theta-15)}{8}\sin\theta\,\mathrm{d}\theta$$

$$= c_1(\rho+P)r^2\left(\frac{4}{21}a_3-\frac{20}{39}a_5\right), \tag{A7}$$

where ψ is the same as in (A4).

APPENDIX B: ENERGY AND MAGNETIC HELICITY

The magnetic helicity is given by equation (13) where, if $\beta(\psi)$ is given by equation (14), $A_{r,\theta}$ and A_r are

$$A_{r,\theta}=\frac{e^{(\lambda-\nu)/2}}{\sin\theta}\psi\zeta_0\left(|\psi/\bar\psi|-1\right)^\sigma\Theta(|\psi/\bar\psi|-1),$$

$$A_r = e^{(\lambda-\nu)/2}\zeta_0\int_0^\theta\frac{\psi}{\sin\theta'}\left(|\psi/\bar\psi|-1\right)^\sigma$$

$$\times\Theta(|\psi/\bar\psi|-1)\mathrm{d}\theta'. \tag{B1}$$

The total energy of the system is $E=M+\delta M$, where M is the mass of the (spherically symmetric) star without magnetic field and δM is the contribution induced by the magnetic field. It can be determined by considering the far-field limit of the space–time metric (Misner et al. 1973; Thorne 1980), in terms of the function $m_0(r)$ defined in equation (C1):

$$\delta M = \lim_{r\to\infty}m_0(r). \tag{B2}$$

The components of the perturbed Einstein's equations relevant for the determination of $m_0(r)$ give, for choice (14) of the function $\beta(\psi)$,

$$m_0' - 4\pi r^2\frac{\rho'}{P'}\delta p_0 = \frac{1}{3}(a_1')^2 e^{-\lambda} + \frac{6}{7}(a_3')^2 e^{-\lambda}$$

$$+\frac{15}{11}(a_5')^2 e^{-\lambda} + \frac{2}{3r^2}a_1^2 + \frac{72}{7r^2}a_3^2 + \frac{450}{11r^2}a_5^2$$

$$+\frac{e^{-\nu}}{4}\left[\int_0^\pi\zeta_0^2\left(|\psi/\bar\psi|-1\right)^{2\sigma}\Theta(|\psi/\bar\psi|-1)\frac{\psi^2}{\sin\theta}\mathrm{d}\theta\right],$$

$$\delta p_0' + \left[\frac{\nu'}{2}\left(\frac{\rho'}{P'}+1\right) + 4\pi r e^\lambda(\rho+P)\right]\delta p_0$$

$$+e^{2\lambda}m_0(\rho+P)\left(\frac{1}{r^2}+8\pi P\right)$$

$$= (\rho+P)\Bigg\{-\frac{2}{3}a_1'\left[c_0 - \frac{4}{5}c_1\left(a_1 - \frac{3}{7}a_3\right)\right]$$

$$-\frac{12}{7}a_3'c_1\left(\frac{2}{15}a_1 - \frac{8}{15}a_3 + \frac{10}{33}a_5\right)$$

$$-\frac{10}{11}a_5'c_1\left(\frac{4}{21}a_3 - \frac{20}{39}a_5\right) - \frac{1}{3r}(a_1')^2 - \frac{6}{7r}(a_3')^2$$

$$-\frac{15}{11r}(a_5')^2 + \frac{2e^\lambda}{3r^3}a_1^2 + \frac{72e^\lambda}{7r^3}a_3^2 + \frac{450e^\lambda}{11r^3}a_5^2$$

$$-\frac{e^{\lambda-\nu}}{4r}\left[\int_0^\pi\zeta_0^2\left(|\psi/\bar\psi|-1\right)^{2\sigma}\Theta(|\psi/\bar\psi|-1)\frac{\psi^2}{\sin\theta}\mathrm{d}\theta\right]\Bigg\} \tag{B3}$$

(where δp_0 is the $l=0$ component of the pressure perturbation).

Finally, the magnetic energy is (Straumann 2004; Paper I)

$$E_m = \frac{1}{2}\int_0^\infty r^2 e^{(\lambda+\nu)/2}\mathrm{d}r\int_0^\pi\sin\theta B^2\mathrm{d}\theta. \tag{B4}$$

The above formula can be used to compute the relative amount of magnetic energy associated with toroidal and poloidal fields.

The equations for choice (15) of the function β can be obtained by the following substitutions: $\psi\zeta_0\to-\beta_0$ in (B1); $\psi^2\zeta^2{}_0\to\beta_0^2$ in (B3).

APPENDIX C: QUADRUPOLE DEFORMATIONS

The perturbed metric can be written as (Ioka & Sasaki 2004; Colaiuda et al. 2008)

$$\mathrm{d}s^2 = -e^\nu\left\{1+2[h_0(r)+h_2(r)P_2(\cos\theta)]\right\}\mathrm{d}t^2$$

$$+2\left[i_1(r)P_1(\cos\theta)+i_2(r)P_2(\cos\theta)+i_3(r)P_3(\cos\theta)\right]\mathrm{d}t\,\mathrm{d}r$$

$$+2\sin\theta\left[v_1\frac{\partial}{\partial\theta}P_1(\cos\theta)+v_2\frac{\partial}{\partial\theta}P_2(\cos\theta)\right.$$

$$\left.+v_3\frac{\partial}{\partial\theta}P_3(\cos\theta)\right]\mathrm{d}t\,\mathrm{d}\phi$$

$$+2\sin\theta\left[w_2\frac{\partial}{\partial\theta}P_2(\cos\theta)+w_3\frac{\partial}{\partial\theta}P_3(\cos\theta)\right]\mathrm{d}r\,\mathrm{d}\phi$$

$$+e^\lambda\left\{1+\frac{2e^\lambda}{r}[m_0(r)+m_2(r)P_2(\cos\theta)]\right\}\mathrm{d}r^2$$

$$+r^2[1+2k_2(r)P_2(\cos\theta)]\left(\mathrm{d}\theta^2+\sin^2\theta\mathrm{d}\phi^2\right). \tag{C1}$$

The quadrupole ellipticity of the star is defined as $\varepsilon_Q = Q/I,^2$ where Q is the mass–energy quadrupole moment, given by the far-field limit of metric (C1):

$$h_2(r\to\infty)\sim Q/r^3, \tag{C2}$$

and I is the mean value of the moment of inertia of the star. The value of I can be estimated from the limit $\Omega\to 0$ of the ratio J/Ω in a slowly rotating star model (Ω is the angular velocity and J is the angular momentum). For $M=1.4\,\mathrm{M_\odot}$ we have $I=98.39\,\mathrm{km^3}$ (APR2 EOS) and $I=134.6\,\mathrm{km^3}$ (GNH3 EOS).

In order to compute ε_Q we need to solve the following system of linearized Einstein equations (here we consider choice 14):

$$k_2' + h_2' - h_2\left(\frac{1}{r}-\frac{\nu'}{2}\right) - m_2\left(\frac{\nu'}{2}+\frac{1}{r}\right)\frac{e^\lambda}{r}$$

$$= \frac{5}{4r^2}\int_0^\pi\psi_{,\theta}\psi_{,r}\frac{(3\cos^2\theta-1)\cot\theta}{\sin\theta}\mathrm{d}\theta, \tag{C3}$$

$$h_2 + \frac{e^\lambda}{r}m_2$$

$$= \frac{5}{4r^2}\int_0^\pi\left[-(\psi_{,r})^2 r^2 e^{-\lambda}+e^{-\nu}\zeta_0^2\psi^2 r^2(|\psi/\bar\psi|-1)^{2\sigma}\right.$$

$$\left.\times\Theta(|\psi/\bar\psi|-1)\right]\frac{(3\cos^2\theta-1)}{\sin\theta}\mathrm{d}\theta, \tag{C4}$$

----

[2] Note that in Colaiuda et al. (2008) equation (81) has a wrong minus sign.

$$\left(v' + \frac{2}{r}\right)k_2' + \frac{2}{r}h_2' - \frac{4}{r^2}e^{\lambda}k_2 - \frac{6}{r^2}e^{\lambda}h_2$$

$$- \left(\frac{1}{r^2} + 8\pi P\right)\frac{2e^{2\lambda}}{r}m_2 - 8\pi e^{\lambda}\delta p_2$$

$$= \frac{5}{4r^4}e^{\lambda}\int_0^{\pi}\Bigg[-(\psi_{,\theta})^2 + (\psi_{,r})^2 r^2 e^{-\lambda}$$

$$+ e^{-v}\zeta_0^2\psi^2 r^2(|\psi/\bar{\psi}| - 1)^{2\sigma}\Theta(|\psi/\bar{\psi}| - 1)\Bigg]$$

$$\times \frac{(3\cos^2\theta - 1)}{\sin\theta}d\theta, \tag{C5}$$

where

$$\psi = \Bigg[-a_1 + \frac{a_3(3 - 15\cos^2\theta)}{2}$$

$$+ \frac{a_5(-315\cos^4\theta + 210\cos^2\theta - 15)}{8}\Bigg]\sin^2\theta.$$

The integration can be simplified by introducing the auxiliary function

$$y_2 = k_2 + h_2 + W(r,\theta), \tag{C6}$$

where

$$W(r,\theta) = \frac{5e^{-\lambda}}{16r^2}\int_0^{\pi}\Big[-e^{\lambda}(\psi_{,\theta})^2 + r^2(\psi_{,r})^2$$

$$- 2r\psi_{,\theta}\psi_{,r}\cot\theta\Big]\frac{(3\cos^2\theta-1)}{\sin\theta}d\theta. \tag{C7}$$

This generalizes the variable change adopted in Ioka & Sasaki (2004), Colaiuda et al. (2008). With the above substitution we are left with two coupled equations

$$y_2' + v'h_2 = W' + \frac{5}{4r^2}\int_0^{\pi}\Bigg\{\psi_{,\theta}\psi_{,r}\cot\theta + \left(\frac{v'}{2} + \frac{1}{r}\right)$$

$$\times\Big[-(\psi_{,r})^2 r^2 e^{-\lambda} + e^{-v}\zeta_0^2\psi^2 r^2(|\psi/\bar{\psi}| - 1)^{2\sigma}$$

$$\times\Theta(|\psi/\bar{\psi}| - 1)\Big]\Bigg\}\frac{(3\cos^2\theta-1)}{\sin\theta}d\theta, \tag{C8}$$

$$h_2' + \frac{4}{v'r^2}e^{\lambda}y_2 + \left[v' - \frac{8\pi e^{\lambda}}{v'}(\rho+P) + \frac{2}{v'r^2}(e^{\lambda}-1)\right]h_2$$

$$= \frac{5}{8r^2}\int_0^{\pi}\Bigg[-v'e^{-\lambda}r^2(\psi_{,r})^2 + 2\psi_{,r}\psi_{,\theta}\cot\theta$$

$$+ e^{-v}\zeta_0^2\psi^2\left(v'r^2 - \frac{2}{v'}e^{\lambda}\right)(|\psi/\bar{\psi}| - 1)^{2\sigma}$$

$$\times\Theta(|\psi/\bar{\psi}| - 1)\Bigg]\frac{(3\cos^2\theta - 1)}{\sin\theta}d\theta$$

$$+ \frac{10\pi}{v'}e^{\lambda}(\rho + P)\int_0^{\pi}[c_0 + c_1\psi]\psi_{,\theta}\sin^2\theta\cos\theta d\theta, \tag{C9}$$

where we have used the following relation (arising from $T^{\theta v}_{;v} = 0$):

$$\delta p_2 = -(\rho + P)\left(h_2 + \frac{5}{4}\int_0^{\pi}[c_0 + c_1\psi]\psi_{,\theta}\sin^2\theta\cos\theta d\theta\right). \tag{C10}$$

Equations (C8) and (C9) can be solved using the same procedure described in Colaiuda et al. (2008). If we adopt choice (15) for the relation between toroidal and poloidal fields, we proceed in the same way. In this case the final system of equations writes

$$y_2' + v'h_2 = W' + \frac{5}{4r^2}\int_0^{\pi}\Bigg\{\psi_{,\theta}\psi_{,r}\cot\theta + \left(\frac{v'}{2} + \frac{1}{r}\right)$$

$$\times\Big[-(\psi_{,r})^2 r^2 e^{-\lambda} + e^{-v}\beta_0^2 r^2(|\psi/\bar{\psi}| - 1)^{2\sigma}$$

$$\times\Theta(|\psi/\bar{\psi}| - 1)\Big]\Bigg\}\frac{(3\cos^2\theta-1)}{\sin\theta}d\theta, \tag{C11}$$

$$h_2' + \frac{4}{v'r^2}e^{\lambda}y_2 + \left[v' - \frac{8\pi e^{\lambda}}{v'}(\rho+P) + \frac{2}{v'r^2}(e^{\lambda}-1)\right]h_2$$

$$= \frac{5}{8r^2}\int_0^{\pi}\Bigg[-v'e^{-\lambda}r^2(\psi_{,r})^2 + 2\psi_{,r}\psi_{,\theta}\cot\theta$$

$$+ e^{-v}\beta_0^2\left(v'r^2 - \frac{2}{v'}e^{\lambda}\right)(|\psi/\bar{\psi}| - 1)^{2\sigma}$$

$$\times\Theta(|\psi/\bar{\psi}| - 1)\Bigg]\frac{(3\cos^2\theta - 1)}{\sin\theta}d\theta$$

$$+ \frac{10\pi}{v'}e^{\lambda}(\rho + P)\int_0^{\pi}[c_0 + c_1\psi]\psi_{,\theta}\sin^2\theta\cos\theta d\theta. \tag{C12}$$